Accepted Article

Article type : Full Length

A thrombin receptor - derived imaging agent detects subclinical arthritis in mice

Beth Friedman, PhD[1], Michael A. Whitney, PhD[1], Elamprakash N. Savariar, PhD[1], Christa Caneda, B.S.[3], Paul Steinbach, B.S. [2], Qing Xiong, B.S.[2], Dina V. Hingorani, PhD [2], Jessica Crisp, PhD[2], Stephen R. Adams, PhD[1], Michael Kenner, B.S.[3], Csilla N. Lippert, MD PhD[1], Quyen T. Nguyen, MD PhD[4], Monica Guma MD PhD[3], Roger Y. Tsien, PhD[1, 2, 5], and Maripat Corr, MD[3]

[1]Department of Pharmacology, [2]Howard Hughes Medical Institute, [3]Division of Rheumatology, Allergy and Immunology, [4]Division of Head and Neck Surgery, and [5]Department of Chemistry and Biochemistry, University of California at San Diego, La Jolla, California

Correspondence to:
Maripat Corr, MD
University of California San Diego
9500 Gilman Dr.
San Diego, CA 92093-0656
Tel: (858) 534-7817
Fax: (858) 534-5270
E-mail: mpcorr@ucsd.edu

Research Support
This project was supported in part by grants CA158448, NS027177-27, R35 NS097265 and 5K08AR064834 from the National Institutes of Health, the Howard Hughes Medical Institute, and the Rheumatology Research Foundation. The funders had no role in study design, data collection and analysis, decision to publish, or preparation of the manuscript.

Quyen T. Nguyen is a scientific advisor to Avelas and is a shareholder. Avelas has licensed the ACPP technology from the University of California. Michael A. Whitney and

This article has been accepted for publication and undergone full peer review but has not been through the copyediting, typesetting, pagination and proofreading process, which may lead to differences between this version and the Version of Record. Please cite this article as doi: 10.1002/art.40316
This article is protected by copyright. All rights reserved.

Accepted Article

Elamprakash N. Savariar are inventors on patent applications for RACPP technology and have received licensing royalties (less than $10,000). No other conflicts of interest, financial, or otherwise are declared by the authors. No commercial support was received.

ABSTRACT

Objective: Functional imaging of synovitis could improve both early detection of rheumatoid arthritis (RA) and long-term outcomes. Motivated by the intersection of inflammation with coagulation protease activation, we examine coagulation protease activities in arthritic mice with a dual fluorescent Ratiometric thrombin-Activatable Cell Penetrating Peptide ($RACPP_{NleTPRSFL}$).

Method: Mice with chronic transgenic K/BxN arthritis, or with arthritis on Day 1 of passive serum transfer induced arthritis (STIA), were imaged *in vivo* for Cy5 em: Cy7 em ratiometric fluorescence from proteolytic cleavage and activation of $RACPP_{NleTPRSFL}$. Joint thickness was measured from Days 0 to 10 in STIA mice. Microscopic localization of fluorescence, enabled by cleavage-evoked release of Cy5 tissue-adhesive fragments, was correlated with immune-reactivity to markers of inflammation. Thrombin dependence of ratiometric fluorescence was tested by *ex vivo* application of $RACPP_{NleTPRSFL}$ and argatroban to cryosections from Day 1 STIA hindpaws.

Results: In chronic arthritis, $RACPP_{NleTPRSFL}$ fluorescence ratios of Cy5:Cy7 em were significantly higher in diseased swollen ankles of K/BxN transgenic mice than in normal ankles. On Day 1 of STIA, high ratio $RACPP_{NleTPRSFL}$ fluorescence in ankles and toes correlated with subsequent joint swelling. Foci of high ratiometric fluorescence localized to inflammation, as demarcated by immune-reactivity for citrullinated histones, macrophages, mast cells and neutrophils, in soft tissue on Day 1 STIA. *Ex vivo*

This article is protected by copyright. All rights reserved.

application of $RACPP_{NleTPRSFL}$ to Day 1 STIA cryosections produced ratiometric fluorescence that was inhibited by argatroban.

Conclusion: $RACPP_{NleTPRSFL}$ activation detects established experimental arthritis and the detection of inflammation by $RACPP_{NleTPRSFL}$ on Day 1 of STIA correlates with disease progression.

The search for biomarkers to diagnose and monitor inflammatory joint diseases, such as rheumatoid arthritis (RA), is ongoing and ranges from analyses of genetics to assays of biological fluids (1). The need for a direct visualization of inflammatory processes in soft tissues of arthritic joints has given impetus for the development of new imaging probes for radiographic, ultrasound and magnetic resonance imaging (MRI) (2, 3). In addition, optical imaging of molecular processes is an emerging field that could complement existing imaging modalities and accelerate therapeutic decision-making.

In murine models of arthritis, near-infrared fluorescence (NIRF) has been used to image inflammation-activated proteases including cathepsins and matrix metalloproteinases (MMPs) (4-6). Coagulation proteases are also promising biological indicators of arthritis (7). In rheumatoid arthritis (RA) thrombin and tissue factor levels are elevated in synovial fluid (8, 9). In addition, genetic and pharmacological approaches that reduce thrombin activity also attenuate inflammation in murine arthritis models (10-14). A role of extravascular activation of thrombin in experimental arthritis has been further demonstrated by thrombin-based release of a pro-drug within arthritic joints (15).

Thrombin has multiple physiological substrates including fibrinogen, factor V, factor VIII, protease-activated receptor (PAR) 1 and PAR4 (7). In its active form,

This article is protected by copyright. All rights reserved.

Accepted Article

thrombin converts fibrinogen to fibrin, and the extravascular fibrin deposits seen within RA biopsy samples (16, 17) may provide a scaffold for the accumulation of inflammatory cells (18). The proteolytic activity of thrombin contributes to inflammation through fibrin independent mechanisms as well, including cleaving complement C5 to the inflammatory cell chemoattractant C5a (10, 19). Although the link between thrombin activation and established inflammation suggests that thrombin sensors could offer physiologic detection of arthritis, little is known about activation and the spatial distribution of active thrombin in soft tissues in early arthritis.

To examine the spatial and temporal activation of thrombin *in vivo* we utilized a previously described ratiometric activatable cell-penetrating peptide (RACPP) that has a linker, norleucine (Nle)-TPRSFL, designed to include a PAR1-like cleavage site for thrombin (20). This linker peptide holds a Cy5 far-red fluorescent donor in proximity to a Cy7 NIRF acceptor via a hairpin loop (20). Cy5 emission is substantially quenched in the intact probe, but upon thrombin cleavage of the linker peptide there is an increase in the Cy5:Cy7 emission (Cy5:Cy7) ratio. Protease cleavage also exposes a polycation domain coupled to Cy5, which enables tissue adhesion, and effectively tags the site of protease activity (21). $RACPP_{NleTPRSFL}$ detects physiological levels of active thrombin by a rapid (minutes) increase of $RACPP_{NleTPRSFL}$ Cy5:Cy7 ratiometric fluorescence in actively clotting blood (20). Clotting-induced increases in ratiometric fluorescence are significantly inhibited by intravenous co-injection of $RACPP_{NleTPRSFL}$ with the thrombin inhibitor, lepirudin (20). Here we test if activation of $RACPP_{NleTPRSFL}$ provides an optical sensor for established and subclinical arthritis, and if acute ratiometric fluorescence correlates with disease progression.

This article is protected by copyright. All rights reserved.

Accepted Article

Accepted Article

MATERIALS AND METHODS

Synthesis of ratiometric activatable cell penetrating peptides. A thrombin cleavable RACPP, (cleavage sequence, (NleTPRSFL)), and a matrix metalloproteinase (MMP) cleavable RACPP, (cleavage sequence, PLGC(Me)AG), were synthesized using standard solid phase Fmoc syntheses, and all peptides were amidated at their C-termini. A control uncleavable probe with a poly(ethyleneglycol) (mPEG) linker of matching length was also synthesized. Detailed syntheses including labeling with Cy5 and Cy7 are previously reported (20, 22).

Mice and *in vivo* arthritis models. Mice were maintained at 21°C ± 2°C on a 12-hour light/dark cycle with food and water ad libitum in the University of California, San Diego (UCSD) animal facility, which is accredited by the American Association for Accreditation of Laboratory Animal Care. This study was performed in strict accordance with the recommendations in the Guide for the Care and Use of Laboratory Animals of the National Institutes of Health. The UCSD Institutional Animal Care and Use Committee approved these experiments.

Spontaneous arthritis. KRN T cell receptor transgenic mice were a gift from Drs. D. Mathis and C. Benoist (Harvard Medical School, Boston, MA and Institut de Génétique et de Biologie Moléculaire et Cellulaire, Strasbourg, France), and were maintained on a C57BL/6 background (K/B) (23). Arthritic mice were obtained by crossing K/B with NOD/Lt (N) animals (K/BxN). Male (n=3) and female (n=6) transgenic and female nontransgenic siblings (n=3) were studied at 8 weeks of age. Additional male transgenic mice were used in pilot studies. Arthritis spontaneously started at approximately five weeks of age and was fully established by eight weeks. These

This article is protected by copyright. All rights reserved.

strains were bred and maintained in the UCSD animal facilities.

Serum transfer induced arthritis (STIA). Arthritic adult K/BxN mice were bled and their sera were pooled. Male C57BL/6 mice were purchased from Charles River (Hollister, CA) and injected at 8-12 weeks of age. C57BL/6 mice were injected with 200µl intraperitoneally (i.p.) on Day 0 (24).

***In vivo* joint swelling measures: Caliper-based or white light photography.** Ankle thickness was measured with a caliper (Mitutoyo America, Aurora, IL). To image toes for swelling, mice were anesthetized and the hindpaws were elevated and attached by adhesive to a glass slide mounted on aluminum posts to allow positioning of the slide on top of the abdomen and exposure of the plantar surfaces of the paws. White light images were obtained with a Nikon D90 camera mounted at a distance of 17.5 cm from the supporting platform and a ruler was used for calibration. Images were exported with Camera Control Pro2 software. Using these images the outline of each toe was drawn, the area assessed by ImageJ and then divided by the length of the toe to obtain the aspect ratio i.e. toe thickness (Supplementary Figures 1 and 2). A series of toe measurements was performed in normal mice to validate that this method normalized for differences in toe length (Supplementary Figure 1).

***In vivo* imaging of ratiometric fluorescence.** Mice were intravenously injected with 10 nmol RACPP in water, while under anesthesia with 2% isoflurane. After two hours the mice were re-anesthetized for white light and fluorescent imaging. Images were obtained using a 2D Maestro™ fluorescence imager (CRI, Woburn MA), engineered with a tunable liquid crystal emission filter. Using Cy5 excitation (620/20 nm), fluorescence was measured across a range of wavelengths (640-840 nm in 10 nm

This article is protected by copyright. All rights reserved.

Accepted Article

steps). For ratio quantitation, the intensities of Cy5 and Cy7 emission were quantified: Cy5 emission was integrated across 660-720 nm and Cy7 values were extracted by integration across a far red range of 760-830 nm using software of local design (20). The software also produced a ratio image (Cy5:Cy7) in which the value of the ratio was depicted in pseudocolor (low ratios from low rates of RACPP cleavage at the blue end of the color bar and high ratios from high rates of proteolytic cleavage at the red end).

Ratiometric fluorescence quantitation. Fixed regions of interest (ROIs) were placed over Maestro™ single channel images of the right and left malleoli (Supplementary Figure 3) or across the entire toe. The integrated intensity of fluorescence in each channel was measured in ImageJ. For each value, background subtraction was performed, which incorporated the camera dark current and autofluorescence. The autofluorescence was calculated from fluorescent imaging of uninjected mice at a series of exposure times.

Histology. For microscopic fluorescent imaging of RACPP that had been cleaved in vivo, hindpaws were embedded in Tissue Tek and frozen in 2-methylbutane that was equilibrated in dry ice and then tissue was stored at -80 °C. Tissue cryosections (15 µm) of hindpaws were directly mounted onto Cryojane tape (Leica) and imaged while on the tape to preserve the structure of undecalcified, unfixed bone. Sections were pre-imaged for ratiometric fluorescence prior to immunostaining at 640 excitation (ex) and 685/40 emission (em) for Cy5 and 785/60 em for Cy7. Immunostaining was then performed with antibodies conjugated to Alexa 488 for cKIT (eBioscience, 11-1171-81), Gr-1 (eBioscience, 11-5931-85), and F4/80 (Abcam 60343-50). Anti-citrullinated histone H3 (Abcam, 5103) was unconjugated and anti-rabbit

This article is protected by copyright. All rights reserved.

Accepted Article

Alexa-488 secondary antibody (Invitrogen, A1108) was used for detection. Antibodies were visualized with 488 nm (ex) and 525/40 nm (em) fluorescence. All images for quantitation were acquired at 0.4 micron/pixel resolution. To assess staining intensity of immuno-tagged inflammatory cells in regions of high and low $RACPP_{NleTPRSFL}$ cleavage, we adapted the microarray profile plugin from ImageJ (Supplementary Figure 4). In brief, 144 individual rectangles (500 pixels each) were placed on ROIs for RACPP (Cy5) and antibody fluorescence (488 nm) for each immunostained section. Paired measures of fluorescent intensities for each channel were obtained for ROIs with high and low Cy5 signal. The fluorescence was normalized to the highest value for each section and the normalized Cy5 and 488 nm immunofluorescence were plotted (n=3 sections across 3 mice). DAPI staining was imaged on a separate series of sections at 405 nm (ex) and 460/60 nm (em). Confocal images were acquired with a Nikon Ti-E microscope.

Ex vivo assay of protease cleavage of $RACPP_{NleTPRSFL}$. Cryosections of tissue harvested from Day 1 arthritic mice were incubated with topically applied 2.5 µM $RACPP_{NleTPRSFL}$, or $RACPP_{PLGC(Me)AG}$. The effect of protease inhibition on $RACPP_{NleTPRSFL}$ cleavage was determined by coincubation of 2.5 µM $RACPP_{NleTPRSFL}$ with 350 µM argatroban (Selleckchem-S2069). Confocal images of adjacent control sections incubated with $RACPP_{NleTPRSFL}$ in the absence of inhibitor were used to locate ROIs with high ratio values (>4) for the Cy5:C7 intensity. The effect of argatroban was determined from adjacent sections using these ROIs (12096 pixel area) with ImageJ. A minimum of 3 section pairs each from 4 mice with Day 1 STIA and from 3 normal control mice were assessed.

This article is protected by copyright. All rights reserved.

Accepted Article

Statistics. Statistical analysis was performed using PRISM software (version 6.0, GraphPad Software Inc., La Jolla, CA). The data are represented as means ± standard errors of the mean (SEM). Pearson correlation coefficients were computed to assess linear relationships. Area under the curve (AUC) from baseline and receiver operator curves (ROC) were calculated using PRISM. One-way ANOVA and Tukey's post hoc test were used for multiple comparisons. Significance was set at $P<0.05$.

RESULTS

RACPP noninvasively identifies joints with established arthritis. Protease-dependent cleavage of $RACPP_{NleTPRSFL}$ has been demonstrated in clotting blood at high spatial and temporal resolution, and the cleavage has been traced to thrombin activity (20). The thrombin inhibitor, argatroban, attenuates symptoms in the K/BxN transgenic (Tg) model of arthritis (10). Hence, we examined the activation and spatial localization of $RACPP_{NleTPRSFL}$ ratiometric fluorescence in this model. Tg mice with measurable ankle swelling and nontransgenic (BxN) sibling mice were injected with $RACPP_{NleTPRSFL}$ and imaged after two hours of probe circulation (Figure 1A). Other Tg mice were injected with an uncleavable probe ($RACPP_{mPEG}$), which has a PEG linker substituted for the cleavable PAR-1 like peptide NleTPRSFL. Higher $RACPP_{NleTPRSFL}$ cleavage is indicated by an increased ratio of Cy5:Cy7 emission, which is displayed as a redder pseudocolor (Figure 1A). High ratiometric fluorescence was observed in the ankles and hindpaws of living Tg mice (Figure 1A). Quantitation showed significantly increased Cy5:Cy7 $RACPP_{NleTPRSFL}$ fluorescence emission ratios in Tg mice relative to sibling controls (mean ± SD: 5.6±0.69 and 2.1±0.56 respectively; $P<0.01$) or to Tg mice tested

This article is protected by copyright. All rights reserved.

Accepted Article

with uncleavable $RACPP_{mPEG}$ (1.6 ±0.46; *P*<0.001) (Figure 1B). The dotted line represents two SD below the mean Cy5:Cy7 $RACPP_{NleTPRSFL}$ emission ratio for arthritic paws.

Ratiometric fluorescence originating from tissue deep to the skin is illustrated by comparison of cryosection fluorescence to an image of a swollen toe with high $RACPP_{NleTPRSFL}$ ratiometric fluorescence (black arrow, Figure 1C), from a Tg mouse. The toe cryosection shows that the *in vivo* high ratio patch stems from articular cartilage and periarticular soft tissue (Figure 1D), while the neighboring toe mirrors the low ratios observed *in vivo* (Figure 1C and D).

$RACPP_{NleTPRSFL}$ predicts subsequent joint swelling. To evaluate the activation of $RACPP_{NleTPRSFL}$ in early arthritis, we chose the STIA model because the onset of arthritis occurs reliably within three days of serum inoculation. Here, male C57BL/6 mice (n=6) were injected with 200µl K/BxN sera on Day 0. On Day 1, mice were injected with 10 nmol $RACPP_{NleTPRSFL}$ and imaged two hours later (Figure 2A and Supplementary Figure 5). Mice were monitored daily (Day 0 to Day 10) for toe and ankle swelling. No measurable ankle swelling was detected on Day 1; however, there was an increase in ankle thickness in some mice on Day 2 with significant swelling attained at Day 3 and continuing to Day 10 (Figure 2B, P<0.05 compared to baseline).

In order to assess a prognostic value of early ratiometric $RACPP_{NleTPRSFL}$ fluorescence on Day 1, we quantified Cy5:Cy7 em ratios for a fixed ROI and compared these values to associated ankle AUCs, as the latter measures report changes in ankle thickness over 10 days. Ankle $RACPP_{NleTPRSFL}$ fluorescence and swelling (AUC) were significantly correlated (Pearson coefficient r=0.71, *P*=0.01). All of the ankles with

This article is protected by copyright. All rights reserved.

Accepted Article

$RACPP_{NleTPRSFL}$ Cy5:Cy7 ratios >4 on Day 1 eventually developed swelling. However, five of the ankles that had relatively low $RACPP_{NleTPRSFL}$ Cy5:Cy7 ratios (<4) in the ankle still developed marked swelling over the ensuing nine days (AUC>5; Figure 2B). To extend comparisons of joint swelling and RACPP uptake to toes, we developed a method to measure cumulative toe swelling based on quantitation from white light images of the plantar surfaces of the hindpaws (Figure 2C, and Supplementary Figures 1 and 2). On Day 1 of STIA, foci of high $RACPP_{NleTPRSFL}$ ratiometric fluorescence were detected (Figure 2 and Supplementary Figures 5 and 6). White light images of toes on Day 1 of STIA did not show any obvious swelling when compared to normal mice (Supplementary Figure 6): however, quantitation of toe thickness from aspect ratios, using magnified images, detected swelling for some toes (Figure 2D left panel). Cumulative toe swelling was quantified using the aspect ratios for all toes, which were serially sampled across 10 days, as illustrated for one hindpaw (Figure 2C and 2D). The AUCs calculated from the toe aspect-ratio data and the $RACPP_{NleTPRSFL}$ fluorescence ratios obtained on Day 1 for all toes were significantly correlated (Figure 2D; Pearson correlation coefficient $r=0.47$, $P<0.001$).

We evaluated ROC plots to further assess if $RACPP_{NleTPRSFL}$ ratiometric fluorescence is predictive of swelling. Digits with AUC of ≥1 were considered as swollen (while AUCs of ≤1 classified as not swollen) based on multiple measures of healthy mice. Ankles for normal wild type C57BL/6 (n=4) injected with 10 nmol $RACPP_{NleTPRSFL}$ served as the unaffected controls and measures from mice with AUC>1 for ankle swelling were considered arthritic. Although the number of mice is small, the areas of the ROC curves suggested the probe was more promising at detecting future ankle

This article is protected by copyright. All rights reserved.

Accepted Article

swelling (area=0.81, *P*<0.001) than digit swelling (area=0.75, *P*=0.002) (Supplementary Figure 7).

In acute arthritis RACPP$_{NleTPRSFL}$ fluorescence localizes mainly to periarticular regions. We examined the tissue localization of increased Cy5:Cy7 ratio of RACPP$_{NleTPRSFL}$ on Day 1 STIA observed *in vivo*. The *in vivo* image (Figure 3A) and cryosections of the same paw (Figure 3B) show regions with high RACPP$_{NleTPRSFL}$ ratiometric fluorescence. In similar regions, the microscopic localization shows high RACPP$_{NleTPRSFL}$ Cy5:Cy7 ratio intensity deep to the skin within juxta-articular soft tissue as well as in scant areas that were not visualized *in vivo* (e.g. digit 5 in Figure 3B). High magnification reveals only a small focus of uptake in cartilage (Figure 3B). Application of a DNA stain, DAPI, in a neighboring section (Figure 3C) showed that the periarticular patch of high ratio periarticular fluorescence is hypercellular with abnormal decondensed DNA-stained nuclei. This contrasts with the relatively sparse DNA staining on the opposite side of the toe in a region of low ratio signal.

RACPP fluorescence co-localizes with inflammatory cells on Day 1 of STIA. We examined the cellular composition of foci with high *in vivo* ratiometric signal in hindpaws from mice (n=3) harvested after *in vivo* RACPP$_{NleTPRSFL}$ imaging on Day 1 of STIA. Toes that demonstrated high ratio cleavage were selected (Figure 4A) for further microscopic examination. Hematoxylin and eosin staining of neighboring sections demonstrated areas of cellular infiltration (Figure 4B, left panel) that mapped to areas of high ratiometric signal (Figure 4B, right panel).

To characterize the cellular infiltrate in areas with high RACPP$_{NleTPRSFL}$ cleavage, we immunostained sections with antibodies that recognize citrullinated histones,

This article is protected by copyright. All rights reserved.

Accepted Article

neutrophils, mast cells, and macrophages (Figure 4C). All antibody markers demonstrate clusters of immuno-labeled cells that intermingle with high $RACPP_{NleTPRSFL}$ ratiometric signal. This co-localization indicates that inflammatory cells in Day 1 STIA hindpaws are situated in active- protease enriched niches (Figure 4C and D). We also immunostained sections with antibodies for citrullinated histones to test if the neutrophil clusters in high cleavage ratio patches were activated, because histone citrullination is a signature of neutrophil extracellular traps (NETs) (25). Citrullinated histone immunostaining intensity significantly correlated with the magnitude of Cy5- tagged ratiometric signal (Figure 4C and D; Pearson coefficient 0.54, $P<0.0001$).

Ex vivo assay for protease dependence of RACPP cleavage in STIA joints. We examined whether RACPP cleavage could detect ex vivo protease activity in tissues from Day 1 mice with STIA, which had not been injected *in vivo* with RACPP. Sites of inflammation were independently identified by immunostaining for citrullinated histones (Figure 5A). Topical application of $RACPP_{NleTPRSFL}$ on cryosections resulted in high ratiometric fluorescence in regions of citrullinated histones (Figure 5A), indicating that the probe itself did not instigate release of nuclear DNA during *in vivo* testing. In contrast to the high ratiometric fluorescence observed with thrombin cleavable $RACPP_{NleTPRSFL}$, topically applied MMP cleavable $RACPP_{PLGC(Me)AG}$ showed low ratiometric signal in the vicinity of citrullinated histones, although higher ratios were detected in the articular cartilage (Figure 5A). The cartilage signal is consistent with prior studies where $RACPP_{PLGC(Me)AG}$ signal was observed in healthy sternal cartilage (Supplementary Figure 8) (22). In the presence of argatroban the ratiometric signal from topically applied $RACPP_{NleTPRSFL}$, on cryosections of paws from Day 1 STIA mice was

This article is protected by copyright. All rights reserved.

Accepted Article

inhibited and thus remained at the baseline observed for non-arthritic mice (Figure 5C and Supplementary Figure 9).

DISCUSSION

We assessed detection of murine joint inflammation in arthritis with a RACPP designed with a peptide NleTPRSFL encompassing the cleavage site of the thrombin receptor, PAR1 (20). High magnitude $RACPP_{NleTPRSFL}$ ratiometric fluorescence (Cy5:Cy7 emission ratios >4, Figure 1B) distinguished swollen joints with established Tg arthritis from unaffected controls. Upon microscopic examination of high ratiometric fluorescence in Tg joints, we observed signal in joint cartilage, synovium and periarticular regions. High magnitude foci of $RACPP_{NleTPRSFL}$ ratiometric fluorescence were also demonstrated in acute arthritis as early as Day 1 of STIA. Notably, these signals were a predictor for subsequent joint swelling in individual ankles and toes. Microscopic examination of joints on Day 1 STIA revealed that foci of high $RACPP_{NleTPRSFL}$ ratiometric fluorescence were largely restricted to periarticular tissues that were densely populated by mast cells, macrophages, neutrophils and neutrophil extracellular traps (NETs). Interestingly, there was little extension of high magnitude $RACPP_{NleTPRSFL}$ fluorescence into the joint space or cartilage. Taken together, the data show that $RACPP_{NleTPRSFL}$ ratiometric fluorescence noninvasively detects established arthritis and predicts clinically significant acute arthritis. The high spatial resolution of $RACPP_{NleTPRSFL}$ also revealed local differences in protease activation in affected joints in acute versus chronic arthritis.

Several features of the $RACPP_{NleTPRSFL}$ probe design facilitated these studies.

This article is protected by copyright. All rights reserved.

Accepted Article

RACPPs report active proteases with a larger dynamic spectral range than single wavelength probes (26), including those that are optically silenced by quenching (6, 15, 27, 28). Dual fluorescence also affords an additional advantage, as uncleaved low ratio fluorescence can be used to confirm the probe's tissue distribution. Thus the high intensity, but low cleavage ratio fluorescence, observed in cartilage on Day 1 of STIA indicates that the low magnitude cleavage ratio is not a result of lack of access of the RACPP to the joint space, but instead, results from lower levels of protease activity. Another advantage is that high Cy5:Cy7 fluorescence ratios were detected after only two hours of in vivo circulation and did not require an extensive washout period. Based on ex vivo inhibition of $RACPP_{NleTPRSFL}$ ratiometric fluorescence by co-application of the thrombin inhibitor argatroban to Day 1 STIA cryosections, we suggest that the rapid *in vivo* accumulation of high $RACPP_{NleTPRSFL}$ ratiometric fluorescence is likely due to probe cleavage by activated thrombin (20), but contributions from other proteases cannot be excluded.

A role for thrombin in disease modulation was previously reported in the K/BxN transgenic mice (10). Building on this observation, we suggest that thrombin activation, reported by $RACPP_{NleTPRSFL}$ ratiometric fluorescence, is localized to periarticular areas in the chronic transgenic and early STIA models. Arthritis initiation in the K/BxN model is hypothesized to stem from the deposition of anti-glucose-6-phosphate isomerase autoantibodies (29) in joint soft tissue (30), and on charged cartilage surfaces (10, 31). This pattern of antibody deposition is paralleled by high magnitude $RACPP_{NleTPRSFL}$ ratiometric fluorescence microscopically detected in hindpaws of K/BxN Tg mice with established arthritis. Somewhat surprisingly, the microscopic foci of high

This article is protected by copyright. All rights reserved.

Accepted Article

$RACPP_{NleTPRSFL}$ ratiometric fluorescence detected in Day 1 STIA hindpaw cryosections were largely excluded from cartilage, although foci could be detected in neighboring periarticular soft tissue. On the other hand the paucity of cartilage ratiometric fluorescence on Day 1 STIA is consistent with findings from structural 3D imaging by MRI that demonstrate enhanced signal in periarticular areas and around tendons on Day 3 in the STIA model (32), but little signal in the joint space itself. Our data suggest that the periarticular tissue swelling localized by MRI is likely accompanied by an influx of inflammatory cells in early STIA. In this regard, $RACPP_{NleTPRSFL}$ ratiometric fluorescence would also likely be more specific for active inflammation than the perivascular pooling of indocyanine green (ICG) (33), which has been approved for clinical use in imaging by the Food and Drug Administration.

Microscopic examination of joint tissues from Day 1 STIA mice indicated that cleaved probe adheres to regions with clusters of mixed inflammatory cells. Recruitment of inflammatory cells in collagen-induced arthritis accompanies early endothelial activation as demonstrated by *in vivo* imaging with NIRF conjugated anti-E selectin antibodies (34). Other *in vivo* imaging approaches using conjugation of fluorophores to antibodies or markers for macrophages and/or phagocytes such as, F4/80 (35), folate (27, 36) and S100a8/9 (37) have previously demonstrated increases in populations of joint inflammatory cells in acute and established arthritis. The present study expands on these findings with the demonstration that the influx of multiple types of inflammatory cells appears to be coordinated and targeted to regions of high $RACPP_{NleTPRSFL}$ ratiometric fluorescence with elevated protease activities.

Previous work with functionally activated probes for myeloperoxidase activity (38)

This article is protected by copyright. All rights reserved.

Accepted Article

Accepted Article

or cleavage by inflammation-associated enzymes such as cathepsins and matrix metalloproteinases (MMPs) (4-6) has allowed monitoring of arthritis progression. Here, we used an alternative approach and imaged mice by injection of $RACPP_{NleTPRSFL}$ before visible swelling (by eye or caliper measure) in the STIA model and then followed individual mice serially for clinical swelling. Ankles that had foci of high magnitude $RACPP_{NleTPRSFL}$ Cy5:Cy7 emission ratios (>4) on Day 1 of STIA, developed sustained caliper measured ankle swelling. However, five of twelve ankles that subsequently developed swelling had low magnitude ratiometric fluorescence (Cy5:C7 ratio <4) on Day 1 of STIA and were considered as false negatives. Several factors may have limited the detection of cleaved probe in these ankles. First the number of views was restricted by the time required to position the mice under anesthesia. Images were captured only from the medial view of the ankles and the plantar views of the paws. Since the lateral aspect and the dorsum of the hindfoot were not imaged, this may have reduced the sensitivity for predicting later swelling. Activation of other proteases in arthritis is dynamically regulated, as suggested by recent observations of MMP12 and 13 in STIA (5) so that sampling thrombin activation at a single 2 hour time point, one day after serum injection, may not detect all areas of future disease.

The STIA model is known to be heavily neutrophil dependent (39) and NETs associated with neutrophil activation are present in the joints (40). The present study demonstrates that both of these markers of inflammation emerge within 24 hours of serum injection and are targeted to synovial and neighboring soft tissues where there is elevated $RACPP_{NleTPRSFL}$ ratiometric fluorescence. The early targeting of inflammatory cells may reflect thrombin activation of complement pathways to yield the neutrophil

This article is protected by copyright. All rights reserved.

chemoattractant C5a independent of C3 (10, 19). Conversely, thrombin is itself generated via tissue factor pathways that are activated by tissue damage and by NETs (41, 42). Thus the present work provides visualization of a spatial overlap between $RACPP_{NleTPRSFL}$ signal intensity and citrullinated histones, which is consistent with a model of a positive feedback between the generation of NETs and thrombin activation (Supplementary Figure 10).

The clinical use of $RACPP_{NleTPRSFL}$ could extend to monitoring other neutrophil predominant forms of arthritis, such as gout (43), or other disease states that are characterized by inflammation and NET formation such as vascular injury from vasculitis (42, 44). Furthermore, in this study there were multiple inflammatory cell types that mapped to the region of high fluorescence intensity, indicating a broader potential than solely detecting neutrophil activity. In a T cell dependent murine multiple sclerosis model, a prior generation probe indicated that thrombin activation preceded onset of neurological signs, increased at disease peak, and correlated deleterious histologic changes, and clinical severity (45). Collectively, the present study suggests that functional imaging with the $RACPP_{NleTPRSFL}$ biosensor could be used to monitor both the development and progression of synovitis and other inflammatory disease states.

ACKNOWLEDGEMENTS

We are grateful to Dr. Nancy Lane for critical review of the manuscript. We appreciate the services provided by the UCSD School of Medicine Microscopy Core that is funded in part by NIH (NS047101). Sadly, Roger Tsien passed away on August 24, 2016. We are grateful for his insights and leadership.

This article is protected by copyright. All rights reserved.

Accepted Article

Accepted Article

REFERENCES

1. Mankia K, Emery P. Preclinical Rheumatoid Arthritis: Progress Toward Prevention. Arthritis Rheumatol. 2016;68:779-88.

2. Tan YK, Ostergaard M, Conaghan PG. Imaging tools in rheumatoid arthritis: ultrasound vs magnetic resonance imaging. Rheumatology (Oxford). 2012;51 Suppl 7:vii36-42.

3. Mountz JM, Alavi A, Mountz JD. Emerging optical and nuclear medicine imaging methods in rheumatoid arthritis. Nat Rev Rheumatol. 2012;8:719-28.

4. Ibarra JM, Jimenez F, Martinez HG, Clark K, Ahuja SS. MMP-Activated Fluorescence Imaging Detects Early Joint Inflammation in Collagen-Antibody-Induced Arthritis in CC-Chemokine Receptor-2-Null Mice, In-Vivo. Int J Inflam. 2011;2011:691587.

5. Lim NH, Meinjohanns E, Bou-Gharios G, Gompels LL, Nuti E, Rossello A, et al. In vivo imaging of matrix metalloproteinase 12 and matrix metalloproteinase 13 activities in the mouse model of collagen-induced arthritis. Arthritis Rheumatol. 2014;66:589-98.

6. Scales HE, Ierna M, Smith KM, Ross K, Meiklejohn GR, Patterson-Kane JC, et al. Assessment of murine collagen-induced arthritis by longitudinal non-invasive duplexed molecular optical imaging. Rheumatology (Oxford). 2016;55:564-72.

7. Danckwardt S, Hentze MW, Kulozik AE. Pathologies at the nexus of blood coagulation and inflammation: thrombin in hemostasis, cancer, and beyond. J Mol Med (Berl). 2013;91:1257-71.

8. Nakano S, Ikata T, Kinoshita I, Kanematsu J, Yasuoka S. Characteristics of the protease activity in synovial fluid from patients with rheumatoid arthritis and osteoarthritis. Clin Exp Rheumatol. 1999;17:161-70.

9. So AK, Varisco PA, Kemkes-Matthes B, Herkenne-Morard C, Chobaz-Peclat V, Gerster JC, et al. Arthritis is linked to local and systemic activation of coagulation and fibrinolysis pathways. J Thromb Haemost. 2003;1:2510-5.

This article is protected by copyright. All rights reserved.

Accepted Article

10. Auger JL, Haasken S, Binstadt BA. Autoantibody-mediated arthritis in the absence of C3 and activating Fcgamma receptors: C5 is activated by the coagulation cascade. Arthritis Res Ther. 2012;14:R269.

11. Flick MJ, Chauhan AK, Frederick M, Talmage KE, Kombrinck KW, Miller W, et al. The development of inflammatory joint disease is attenuated in mice expressing the anticoagulant prothrombin mutant W215A/E217A. Blood. 2011;117:6326-37.

12. Marty I, Peclat V, Kirdaite G, Salvi R, So A, Busso N. Amelioration of collagen-induced arthritis by thrombin inhibition. J Clin Invest. 2001;107:631-40.

13. Varisco PA, Peclat V, van Ness K, Bischof-Delaloye A, So A, Busso N. Effect of thrombin inhibition on synovial inflammation in antigen induced arthritis. Ann Rheum Dis. 2000;59:781-7.

14. Yang YH, Hall P, Little CB, Fosang AJ, Milenkovski G, Santos L, et al. Reduction of arthritis severity in protease-activated receptor-deficient mice. Arthritis Rheum. 2005;52:1325-32.

15. Gabriel D, Lange N, Chobaz-Peclat V, Zuluaga MF, Gurny R, van den Bergh H, et al. Thrombin-sensitive dual fluorescence imaging and therapeutic agent for detection and treatment of synovial inflammation in murine rheumatoid arthritis. J Control Release. 2012;163:178-86.

16. Chapuy-Regaud S, Sebbag M, Baeten D, Clavel C, Foulquier C, De Keyser F, et al. Fibrin deimination in synovial tissue is not specific for rheumatoid arthritis but commonly occurs during synovitides. J Immunol. 2005;174:5057-64.

17. Clemmensen I, Holund B, Andersen RB. Fibrin and fibronectin in rheumatoid synovial membrane and rheumatoid synovial fluid. Arthritis Rheum. 1983;26:479-85.

18. Sanchez-Pernaute O, Largo R, Calvo E, Alvarez-Soria MA, Egido J, Herrero-Beaumont G. A fibrin based model for rheumatoid synovitis. Ann Rheum Dis. 2003;62:1135-8.

This article is protected by copyright. All rights reserved.

19. Huber-Lang M, Sarma JV, Zetoune FS, Rittirsch D, Neff TA, McGuire SR, et al. Generation of C5a in the absence of C3: a new complement activation pathway. Nat Med. 2006;12:682-7.

20. Whitney M, Savariar EN, Friedman B, Levin RA, Crisp JL, Glasgow HL, et al. Ratiometric activatable cell-penetrating peptides provide rapid in vivo readout of thrombin activation. Angew Chem Int Ed Engl. 2013;52:325-30.

21. Jiang T, Olson ES, Nguyen QT, Roy M, Jennings PA, Tsien RY. Tumor imaging by means of proteolytic activation of cell-penetrating peptides. Proc Natl Acad Sci U S A. 2004;101:17867-72.

22. Savariar EN, Felsen CN, Nashi N, Jiang T, Ellies LG, Steinbach P, et al. Real-time in vivo molecular detection of primary tumors and metastases with ratiometric activatable cell-penetrating peptides. Cancer Res. 2013;73:855-64.

23. Kouskoff V, Korganow AS, Duchatelle V, Degott C, Benoist C, Mathis D. Organ-specific disease provoked by systemic autoimmunity. Cell. 1996;87:811-22.

24. Choe JY, Crain B, Wu SR, Corr M. Interleukin 1 receptor dependence of serum transferred arthritis can be circumvented by toll-like receptor 4 signaling. J Exp Med. 2003;197:537-42.

25. Wang Y, Li M, Stadler S, Correll S, Li P, Wang D, et al. Histone hypercitrullination mediates chromatin decondensation and neutrophil extracellular trap formation. J Cell Biol. 2009;184:205-13.

26. Jaffer FA, Tung CH, Gerszten RE, Weissleder R. In vivo imaging of thrombin activity in experimental thrombi with thrombin-sensitive near-infrared molecular probe. Arterioscler Thromb Vasc Biol. 2002;22:1929-35.

27. Chen WT, Mahmood U, Weissleder R, Tung CH. Arthritis imaging using a near-infrared fluorescence folate-targeted probe. Arthritis Res Ther. 2005;7:R310-7.

This article is protected by copyright. All rights reserved.

Accepted Article

28. Page MJ, Lourenco AL, David T, LeBeau AM, Cattaruzza F, Castro HC, et al. Non-invasive imaging and cellular tracking of pulmonary emboli by near-infrared fluorescence and positron-emission tomography. Nat Commun. 2015;6:8448.

29. Matsumoto I, Staub A, Benoist C, Mathis D. Arthritis provoked by linked T and B cell recognition of a glycolytic enzyme. Science. 1999;286:1732-5.

30. Wipke BT, Wang Z, Kim J, McCarthy TJ, Allen PM. Dynamic visualization of a joint-specific autoimmune response through positron emission tomography. Nat Immunol. 2002;3:366-72.

31. Studelska DR, Mandik-Nayak L, Zhou X, Pan J, Weiser P, McDowell LM, et al. High affinity glycosaminoglycan and autoantigen interaction explains joint specificity in a mouse model of rheumatoid arthritis. J Biol Chem. 2009;284:2354-62.

32. Rose S, Waters EA, Haney CR, Meade CT, Perlman H. High-resolution magnetic resonance imaging of ankle joints in murine arthritis discriminates inflammation and bone destruction in a quantifiable manner. Arthritis Rheum. 2013;65:2279-89.

33. Werner SG, Langer HE, Ohrndorf S, Bahner M, Schott P, Schwenke C, et al. Inflammation assessment in patients with arthritis using a novel in vivo fluorescence optical imaging technology. Ann Rheum Dis. 2012;71:504-10.

34. Gompels LL, Madden L, Lim NH, Inglis JJ, McConnell E, Vincent TL, et al. In vivo fluorescence imaging of E-selectin: quantitative detection of endothelial activation in a mouse model of arthritis. Arthritis Rheum. 2011;63:107-17.

35. Hansch A, Frey O, Sauner D, Hilger I, Haas M, Malich A, et al. In vivo imaging of experimental arthritis with near-infrared fluorescence. Arthritis Rheum. 2004;50:961-7.

36. Kelderhouse LE, Robins MT, Rosenbalm KE, Hoylman EK, Mahalingam S, Low PS. Prediction of Response to Therapy for Autoimmune/Inflammatory Diseases Using an Activated Macrophage-Targeted Radioimaging Agent. Mol Pharm. 2015;12:3547-55.

This article is protected by copyright. All rights reserved.

Accepted Article

Accepted Article

37. Vogl T, Eisenblatter M, Voller T, Zenker S, Hermann S, van Lent P, et al. Alarmin S100A8/S100A9 as a biomarker for molecular imaging of local inflammatory activity. Nat Commun. 2014;5:4593.

38. Gross S, Gammon ST, Moss BL, Rauch D, Harding J, Heinecke JW, et al. Bioluminescence imaging of myeloperoxidase activity in vivo. Nat Med. 2009;15:455-61.

39. Wipke BT, Allen PM. Essential role of neutrophils in the initiation and progression of a murine model of rheumatoid arthritis. J Immunol. 2001;167:1601-8.

40. Rohrbach AS, Hemmers S, Arandjelovic S, Corr M, Mowen KA. PAD4 is not essential for disease in the K/BxN murine autoantibody-mediated model of arthritis. Arthritis Res Ther. 2012;14:R104.

41. Kambas K, Mitroulis I, Apostolidou E, Girod A, Chrysanthopoulou A, Pneumatikos I, et al. Autophagy mediates the delivery of thrombogenic tissue factor to neutrophil extracellular traps in human sepsis. PLoS One. 2012;7:e45427.

42. Kambas K, Chrysanthopoulou A, Vassilopoulos D, Apostolidou E, Skendros P, Girod A, et al. Tissue factor expression in neutrophil extracellular traps and neutrophil derived microparticles in antineutrophil cytoplasmic antibody associated vasculitis may promote thromboinflammation and the thrombophilic state associated with the disease. Ann Rheum Dis. 2014;73:1854-63.

43. Schauer C, Janko C, Munoz LE, Zhao Y, Kienhofer D, Frey B, et al. Aggregated neutrophil extracellular traps limit inflammation by degrading cytokines and chemokines. Nat Med. 2014;20:511-7.

44. Sangaletti S, Tripodo C, Chiodoni C, Guarnotta C, Cappetti B, Casalini P, et al. Neutrophil extracellular traps mediate transfer of cytoplasmic neutrophil antigens to myeloid dendritic cells toward ANCA induction and associated autoimmunity. Blood. 2012;120:3007-18.

45. Davalos D, Baeten KM, Whitney MA, Mullins ES, Friedman B, Olson ES, et al. Early detection of thrombin activity in neuroinflammatory disease. Ann Neurol. 2014;75:303-8.

This article is protected by copyright. All rights reserved.

Accepted Article

FIGURES LEGENDS

Figure 1. *In vivo* imaging of established arthritis with $RACPP_{NleTPRSFL}$. (**A**) $RACPP_{NleTPRSFL}$ cleavage yields high ratio Cy5:Cy7 em fluorescence in a Tg arthritic mouse. This contrasts with the low ratiometric fluorescence, imaged in the ankle of a control sibling injected with $RACPP_{NleTPRSFL}$ or in an ankle of a Tg mouse injected with control probe ($RACPP_{mPEG}$). (**B**) Tg mice (n=6) had significantly higher $RACPP_{NleTPRSFL}$ Cy5:Cy7 emission ratios than siblings (n=5, $P<0.01$), or $RACPP_{mPEG}$ injected Tg mice (n=3; $P<0.001$). (**C**) Focus of high $RACPP_{NleTPRSFL}$ Cy5:Cy7 em in toe (arrow) of transgenic mouse. (**D**) Cryosection from this toe shows signals in articular cartilage and periarticular soft tissue.

Figure 2. *In vivo* detection of Day 1 STIA with $RACPP_{NleTPRSFL}$. (**A**) *In vivo* image of ankles from one mouse demonstrates foci of high $RACPP_{NleTPRSFL}$ Cy5:Cy7 em on Day 1 STIA. (**B**) Significant ankle swelling for the cohort (n=6 mice) did not begin until Day 3. Day 1 $RACPP_{NleTPRSFL}$ Cy5:Cy7 em ratios correlate with AUCs of individual ankle thicknesses integrated over 10 days (Pearson coefficient r=0.71, P=0.01). (**C**) White light images of plantar view of the left hindpaw at baseline, days 1 and 8 of STIA and corresponding ratiometric fluorescence on STIA day 1. (**D**) Daily toe aspect ratios from this paw are plotted (left) and toe with high ratio $RACPP_{NleTPRSFL}$ on Day 1 also demonstrates subsequent sustained swelling (top trace). Scatter plot of $RACPP_{NleTPRSFL}$ Cy5:Cy7 em fluorescence ratios on Day 1 versus the AUCs from serially determined aspect ratios of toe thickness for the complete cohort of 60 toes (n=6 mice) (Pearson correlation coefficient r=0.45, P=0.0003).

This article is protected by copyright. All rights reserved.

Accepted Article

Figure 3. Microscopic localization of *in vivo* cleavage of $RACPP_{NleTPRSFL}$ on Day 1 of STIA in mouse hindpaw. (**A**) Foci of elevated Cy5:Cy7 em on medial aspect of digits 1 and 2. (**Bi**) Cryosection of this hindpaw demonstrates fluorescence on medial surfaces. (**Bii** and **Biii**) Digit 1 shows sparse cartilage label in contrast with predominant peri-articular ratiometric fluorescence. Red and blue boxes define peri-articular sites with high or low ratiometric fluorescence, respectively. (**Ci**) DAPI staining from same hindpaw illustrates increased cellularity in a high ratiometric fluorescent zone (red box), as compared to a low zone (blue box). (**Cii**) Densely cellular zone (red box) is populated with de-condensed nuclei and DNA extrusions. (**Ciii**) Blue-box region of low ratiometric fluorescence shows lower cellularity and DAPI nuclei are sharply condensed.

Figure 4. $RACPP_{NleTPRSFL}$ *in vivo* ratiometric fluorescence on Day 1 of STIA in relation to cellular inflammation. (**A**) Focal high Cy5:Cy7 em on Day 1 *in vivo*. (**B**) On cryosection this toe shows densely stained (H&E) cell infiltrates mapping to foci of high Cy5:Cy7 em. (**C**) Dual channel images of Cy5 for $RACPP_{NleTPRSFL}$ and 488 nm immunolabelling for citrinullated histone (H3), cKIT, F4/80, or Gr-1 to image post-translationally modified histones, mast cells, macrophages or neutrophils respectively. (**D**) Scatter plot quantification of dual channel overlap (n=3 mice). Pearson correlation (r), and *P* values were: citrinullated histone (r=0.54, $P<0.0001$) cKIT (r=0.79, $P<0.0001$); F4/80 (r=0.68, $P< 0.0001$); and Gr-1 (r=0.81, $P<0.0001$) respectively.

This article is protected by copyright. All rights reserved.

Figure 5. Thrombin inhibitor, argatroban, inhibits cleavage of $RACPP_{NleTPRSFL}$ ex vivo in cryosections from Day 1 STIA hindpaws. (**A**) Citrullinated histone (H3) immunofluorescence (left panel) overlaps with $RACPP_{NleTPRSFL}$ fluorescence on cryosection from STIA Day 1 mouse (middle panel). In contrast signal from a MMP sensor ($RACPP_{PLGC(Me)AG}$) does not overlap densely immunostained citrullinated histone positive-regions (right panel). (**B**) Co-incubation of $RACPP_{NleTPRSFL}$ with argatroban reduces $RACPP_{NleTPRSFL}$ fluorescence in inflamed citrullinated histone positive regions. (**C**) Quantitation of effects of thrombin inhibition by co-incubation of topical argatroban and $RACPP_{NleTPRSFL}$. Argatroban reduces Cy5:Cy7 em to levels observed in healthy (Day 0) mice ($P< 0.0001$, one-way ANOVA with Dunnett's *post hoc* test). Scale bars are 100µm.

Accepted Article

This article is protected by copyright. All rights reserved.

Accepted Article

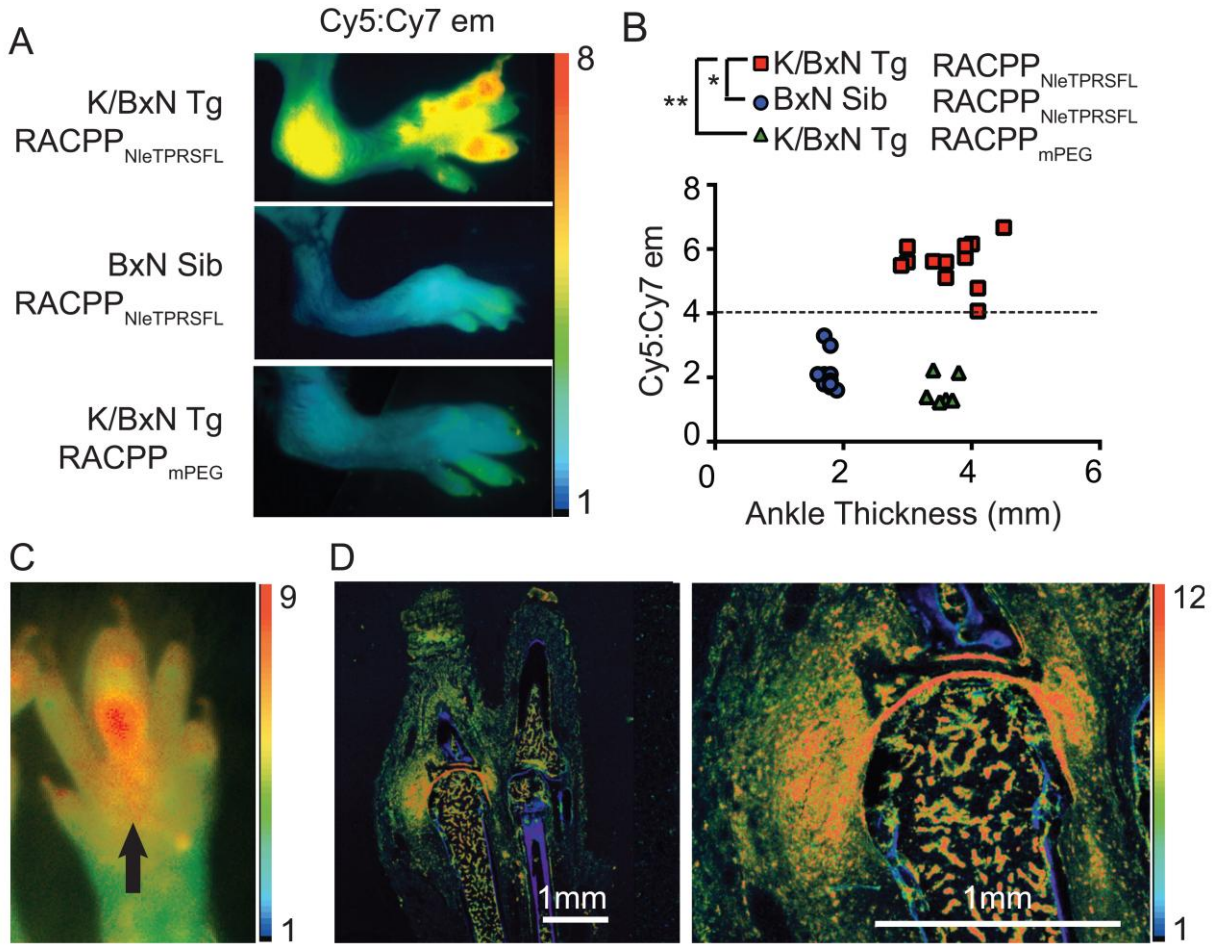

This article is protected by copyright. All rights reserved.

Accepted Article

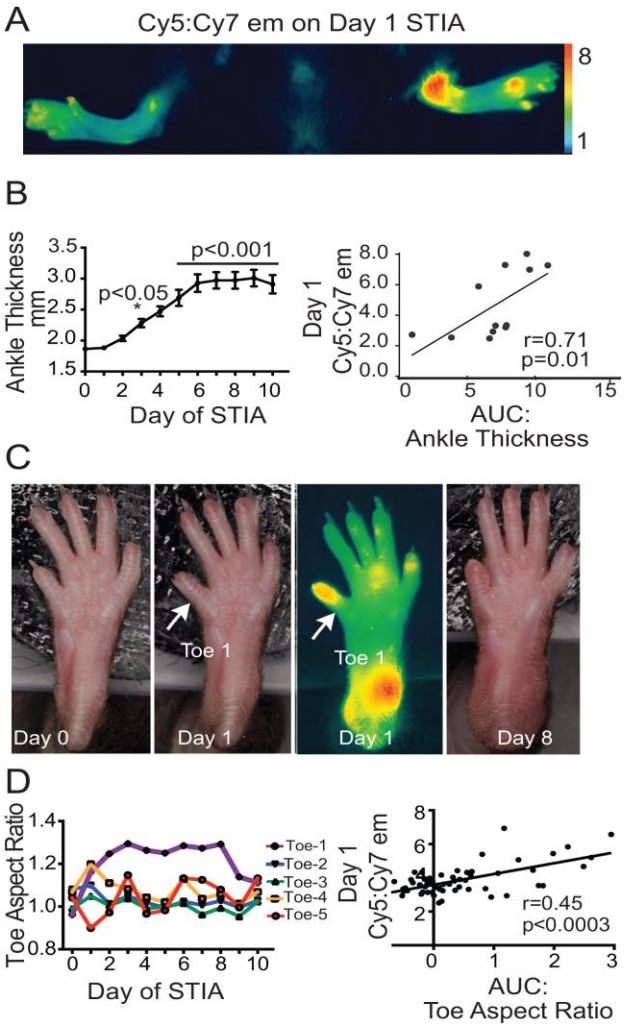

This article is protected by copyright. All rights reserved.

Accepted Article

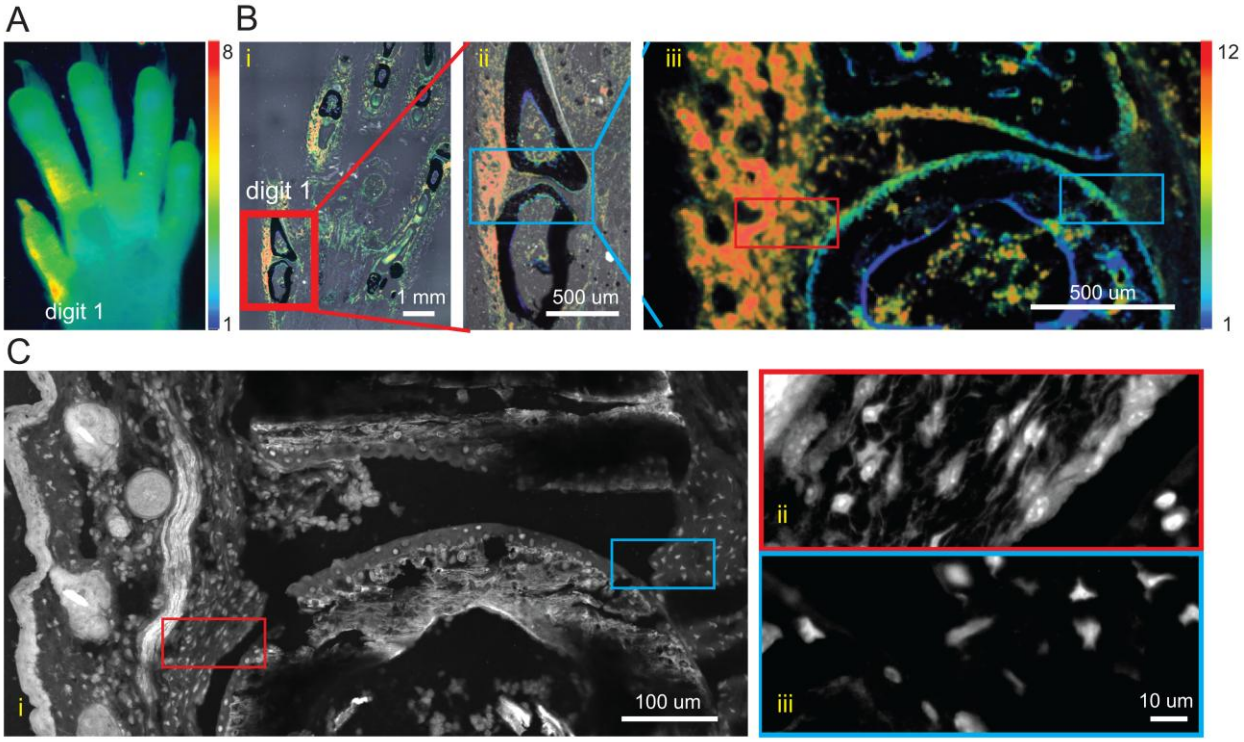

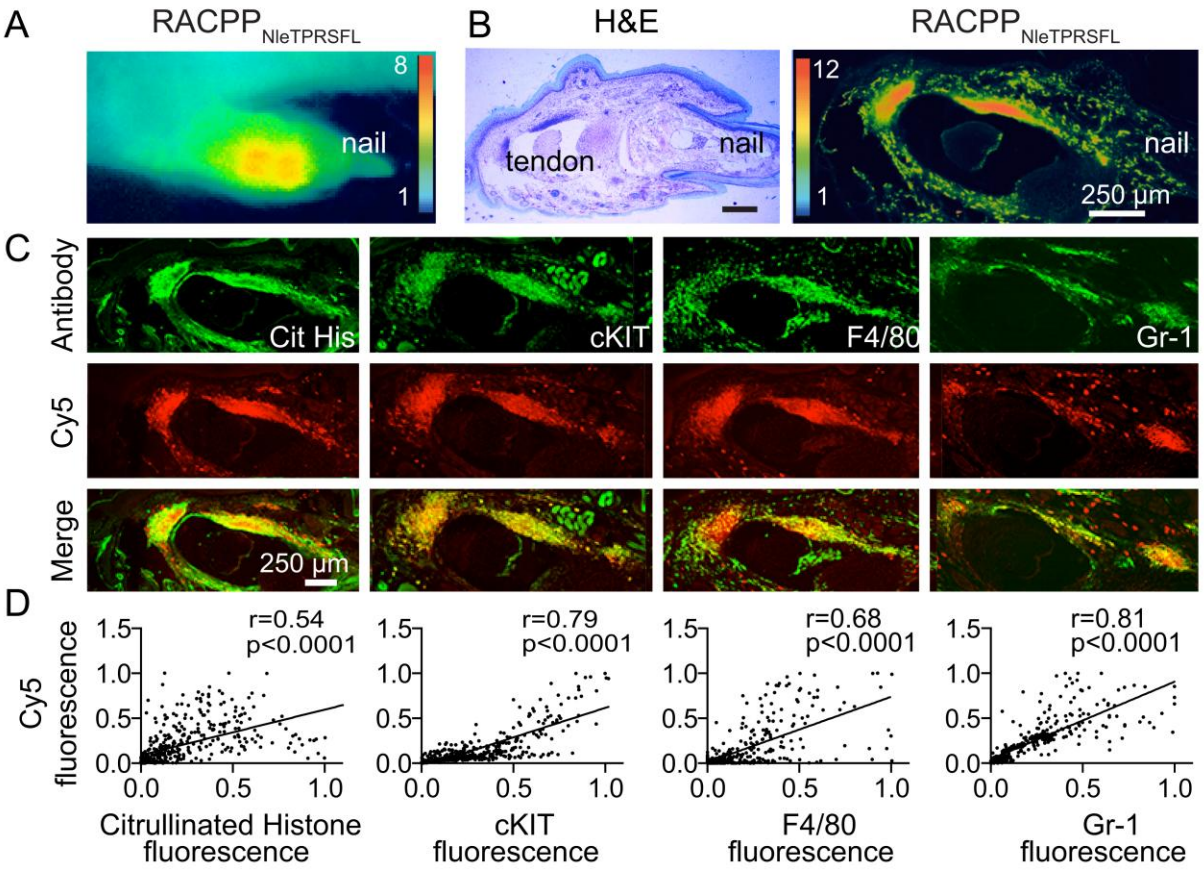

This article is protected by copyright. All rights reserved.

Accepted Article

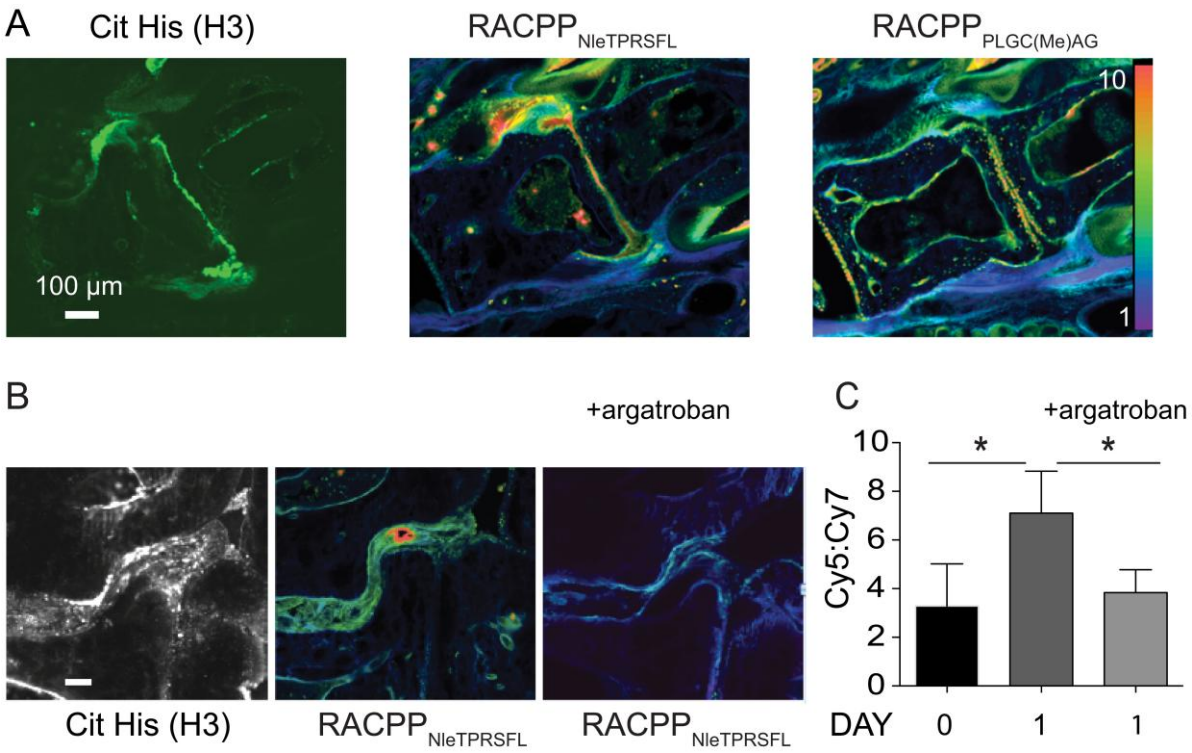

This article is protected by copyright. All rights reserved.